Compton profiles of aluminium corrected by the electron correlation effect

2000 J. Phys.: Condens. Matter 12 9725

(http://iopscience.iop.org/0953-8984/12/47/301)

J. Phys.: Condens. Matter **12** (2000) 9725–9734. Printed in the UK PII: S0953-8984(00)13442-3

Compton profiles of aluminium corrected by the electron correlation effect

S Wakoh†, M Matsumoto† and M Tokii‡

† University of Library and Information Science, Tsukuba-shi, Ibaraki 305-8550, Japan
‡ Gakushuin University, Mejiro, Toshima-ku, Tokyo 171-8588, Japan

Received 25 April 2000, in final form 16 October 2000

Abstract. Directional Compton profiles of face-centred cubic Al are calculated by the augmented-plane-wave method and compared with experimental ones. In general, a theoretical Compton profile which is based upon the IPM (independent-particle model) is a little greater than the experimental one around the origin of the momentum space. In this work, correlation effects are introduced into the results of IPM band calculations and the agreement of theory and experiment is improved very much.

1. Introduction

The Compton effect was discovered by Arthur Compton in 1923. It is a Doppler broadening of inelastically scattered x-ray or γ-ray radiation. The backward scattering of the effect gives the Compton profile which provides information about the initial momentum distribution of the recoiled electrons. That is,

$$J(q_z) = \int\int N(\boldsymbol{q})\,\mathrm{d}q_x\,\mathrm{d}q_y \tag{1}$$

where $N(\boldsymbol{q})$ is the electron momentum density [1]. In the IPM (independent-particle model) the momentum density is given by the following equation:

$$N(\boldsymbol{q}) = \sum_{E_i \leqslant E_\mathrm{F}} \rho_i(\boldsymbol{q}; E_i) = \sum_{E_i \leqslant E_\mathrm{F}} |\chi_i(\boldsymbol{q}; E_i)|^2 \tag{2}$$

where $\rho_i(\boldsymbol{q}; E_i)$ is the momentum density of the state i with energy E_i and $\chi_i(\boldsymbol{q}; E_i)$ is the momentum wave function, and the summation runs over all states whose energies are below the Fermi energy. In the non-interacting electron gas system, the momentum density of the state within the Fermi sphere is unity and outside the Fermi sphere it is zero, i.e.

$$\rho_i(\boldsymbol{q}) = \begin{cases} \delta(q - q_i) & |q| \leqslant q_\mathrm{F} \\ 0 & |q| > q_\mathrm{F} \end{cases} \tag{3}$$

where q_F denotes the Fermi momentum. The Compton profile for the non-interacting electron gas system is, therefore, simply an inverted parabola as illustrated in figure 1, i.e.

$$J(q_z) \propto \begin{cases} q_\mathrm{F}^2 - q_z^2 & q_z \leqslant q_\mathrm{F} \\ 0 & q_z > q_\mathrm{F}. \end{cases} \tag{4}$$

It is well known [2] that electron interaction in an electron gas system has the effect of modifying the occupation numbers $n(q)$ in such a way that the states at $q > q_\mathrm{F}$ become partially occupied,

0953-8984/00/479725+10$30.00

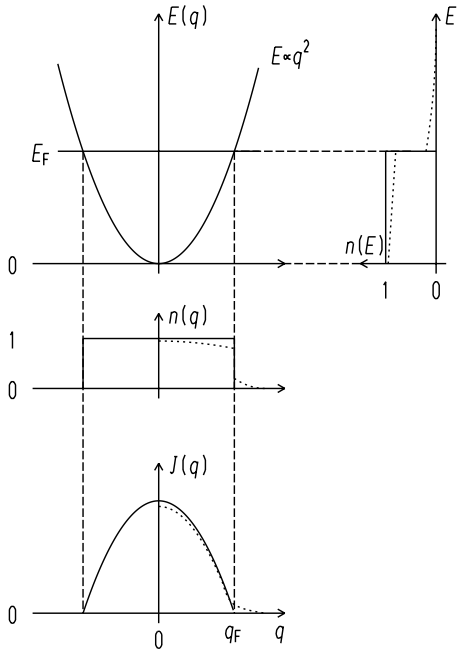

Figure 1. A schematic figure showing the relation between the energy dispersion curve $E(q)$ and the Compton profile $J(q)$ for an electron gas system together with that between the momentum occupation function $n(q)$ and the energy occupation function $n(E)$. The dotted lines show $n(q)$, $n(E)$ and $J(q)$ with the correlation effect. E_{F} denotes the Fermi energy and q_{F} the Fermi momentum.

as shown by the dotted curves in figure 1. Consequently Lundqvist and Lyden [3] introduced the notion that the Compton profile $J(q)$ for an interacting electron gas system is lowered in the region of small momentum and raised to non-zero values for momenta greater than the Fermi momentum, as shown in the figure. Nevertheless, there are no drastic effects of electron correlation and in fact equation (4) is good to a first approximation. In fact, Kubo *et al* [4] estimated the Compton profiles for Al without the electron correlation effect by the APW method and obtained a fairly good agreement with experiments especially as regards the anisotropy. Recently, however, the accuracy of experimental data has been improved very much and the effect can be discussed numerically. So far, correlation effects on Compton profiles have been estimated by using the Lam–Platzman correction [5] for some transition metals, by introducing the momentum occupation function $n(p)$ for a correlated electron gas system for Be [6] and Mg [7], by introducing the phenomenological energy-dependent occupation probability function $n(E)$ for Cr and V [8], and by an elaborate first-principles calculation of the spectral function within the GW-approximation for lithium and sodium [9]. Recently, Matsumoto *et al* [10] estimated the Compton profiles for Mg by the APW method and compared the results with those of the experiments performed by Garreau and Loupias [11] whose FWHM (full width of half-maximum) was 0.2 au. When the electron correlation effect was introduced using the actual electron-density parameter of Mg, i.e. $r_s = 2.66$ au, the agreement with experiments was improved very much but still some disagreement persisted.

Very recently, Sourtti *et al* [12] measured the Compton profiles for Al and studied the electron correlation effects using the Lam–Platzman correction. A good fit was obtained when they used a suitable value for the break at the Fermi momentum. The Lam–Platzman correction

is, however, isotropic and cannot applied to the directional difference of the Compton profiles. Ohata [13] also measured the Compton profiles for Al using synchrotron radiation whose FWHM was 0.1 au. In this paper we estimate the electron–electron correlation effect on the Compton profiles due to the conduction electrons of Al and make comparisons between the available experimental profiles obtained by Ohata and the theoretical ones with a correlation correction.

2. Method of calculation

A self-consistent potential of fcc Al is determined by the conventional APW method within the LDA (local density approximation). The value of the lattice constant a used is 7.6517 au. The energy values and wave functions are calculated at 505 k-points in one 48th of the fcc BZ (Brillouin zone). The 505 k-points make a cubic mesh. The edge length of each cube is a 16th of the distance between Γ and H. In order to determine the eigenfunctions, about one hundred APWs are used in the expansion of the wave functions outside the muffin-tin spheres (interstitial region), and the wave functions inside a muffin-tin sphere whose radius is r_i are expanded up to $l = 4$, where l denotes the angular momentum quantum number. The eigenfunction $\psi_{b,\boldsymbol{k}}(\boldsymbol{r}; E)$ with the eigen-energy E thus determined is expressed as

$$\psi_{b,\boldsymbol{k}}(\boldsymbol{r}; E) \propto \begin{cases} \mathrm{e}^{\mathrm{i}\boldsymbol{k}\cdot\boldsymbol{R}_n} \displaystyle\sum_{lm} \mathrm{i}^l B_{lm,b,\boldsymbol{k}} R_l(|\boldsymbol{r} - \boldsymbol{R}_n|; E) Y_{lm}(\boldsymbol{r} - \boldsymbol{R}_n) & |\boldsymbol{r} - \boldsymbol{R}_n| \leqslant r_i \\ \displaystyle\sum_{\boldsymbol{K}_n} A_{b,\boldsymbol{k}}^{\boldsymbol{K}_n} \mathrm{e}^{\mathrm{i}\boldsymbol{k}+\boldsymbol{K}_n\cdot\boldsymbol{r}} & \text{interstitial region} \end{cases} \tag{5}$$

which is normalized to unity, i.e.

$$\int |\psi_{b,\boldsymbol{k}}(\boldsymbol{r}; E)|^2 \, \mathrm{d}^3 r = 1.0. \tag{6}$$

Here the coefficients A and B are to be determined by the APW equation. The momentum wave function is a Fourier transform of the eigenfunction defined by the formula

$$\chi_{b,\boldsymbol{k}}(\boldsymbol{q}; E) = (2\pi)^{-3/2} \int \psi_{b,\boldsymbol{k}}(\boldsymbol{r}; E) \mathrm{e}^{-\mathrm{i}\boldsymbol{q}\cdot\boldsymbol{r}} \, \mathrm{d}^3 r \tag{7}$$

which is also normalized to unity, i.e.

$$\int |\chi_{b,\boldsymbol{k}}(\boldsymbol{q}; E)|^2 \, \mathrm{d}^3 q = 1.0. \tag{8}$$

The momentum wave function obtained from the APW can be written as the sum of the functions $\chi_b(\boldsymbol{k} + \boldsymbol{K}_n; E)$, i.e.

$$\chi_{b,\boldsymbol{k}}(\boldsymbol{q}; E) = \sum_{\boldsymbol{K}_n} \delta_{\boldsymbol{q},\boldsymbol{k}+\boldsymbol{K}_n} \chi_b(\boldsymbol{k} + \boldsymbol{K}_n; E). \tag{9}$$

The summation over $\boldsymbol{K}_n$ runs over the 1459 reciprocal-lattice vectors in this study. The momentum density $\rho_b(\boldsymbol{k} + \boldsymbol{K}_n; E)$ at each q-point ($\boldsymbol{q} = \boldsymbol{k} + \boldsymbol{K}_n$) for up to the ninth band is obtained from $|\chi_b(\boldsymbol{k} + \boldsymbol{K}_n; E)|^2$. Without the correlation effect, the momentum-density distribution is obtained from

$$N(\boldsymbol{q}) = \sum_b \sum_{E \leqslant E_\mathrm{F}} \rho_b(\boldsymbol{q}; E). \tag{10}$$

The Compton profiles are computed by integrating $N(\boldsymbol{q})$ over a series of planes corresponding to different momenta q_z as shown in equation (1). These integrations are carried out by counting the momentum densities on each plane whose values are obtained at 64 k-points

in each cube by a linear interpolation procedure. The cube is divided into eight smaller cubes. Within each smaller cube, the parameters for the linear functions for the energy eigenvalue and momentum density:

$$E(\boldsymbol{k}) = e_x k_x + e_y k_y + e_z k_z + e_0 \tag{11}$$

$$\rho(\boldsymbol{q}) = \rho_x q_x + \rho_y q_y + \rho_z q_z + \rho_0 \tag{12}$$

are determined by using the values at the four corners of the smaller cube. The procedure for the integration of, for example, $J(q_z)$ along the $\langle 100 \rangle$ direction is as follows. Figure 2 shows the (001) cross section of the repeated-zone scheme for fcc BZ. A $\boldsymbol{k}$-point in the first BZ is denoted by a large dot and some $(\boldsymbol{k} + \boldsymbol{K}_n)$-points are denoted by small dots. The integration is carried out only within one 48th of each BZ instead of the whole BZ by altering the equation, i.e.

$$\begin{aligned} J(q_z) &= \sum_{b,\boldsymbol{K}_n} \delta_{\boldsymbol{q},\boldsymbol{k}+\boldsymbol{K}_n} \int\int_{1\text{st BZ}} \rho_b(\boldsymbol{k}+\boldsymbol{K}_n;\, E)\, \mathrm{d}k_x\, \mathrm{d}k_y \\ &= 8\{J_{(100)}(q) + J_{(010)}(q) + J_{(001)}(q)\}. \end{aligned} \tag{13}$$

Here

$$\begin{aligned} J_{(100)}(q) &= \sum_{b,\boldsymbol{K}_n} \delta_{q,|\boldsymbol{k}+\boldsymbol{K}_n|} \int\int_{1/48\,\text{BZ}} \rho_b(\boldsymbol{k}+\boldsymbol{K}_n;\, E)\, \mathrm{d}k_y\, \mathrm{d}k_z \\ J_{(010)}(q) &= \sum_{b,\boldsymbol{K}_n} \delta_{q,|\boldsymbol{k}+\boldsymbol{K}_n|} \int\int_{1/48\,\text{BZ}} \rho_b(\boldsymbol{k}+\boldsymbol{K}_n;\, E)\, \mathrm{d}k_z\, \mathrm{d}k_x \\ J_{(001)}(q) &= \sum_{b,\boldsymbol{K}_n} \delta_{q,|\boldsymbol{k}+\boldsymbol{K}_n|} \int\int_{1/48\,\text{BZ}} \rho_b(\boldsymbol{k}+\boldsymbol{K}_n;\, E)\, \mathrm{d}k_x\, \mathrm{d}k_y. \end{aligned} \tag{14}$$

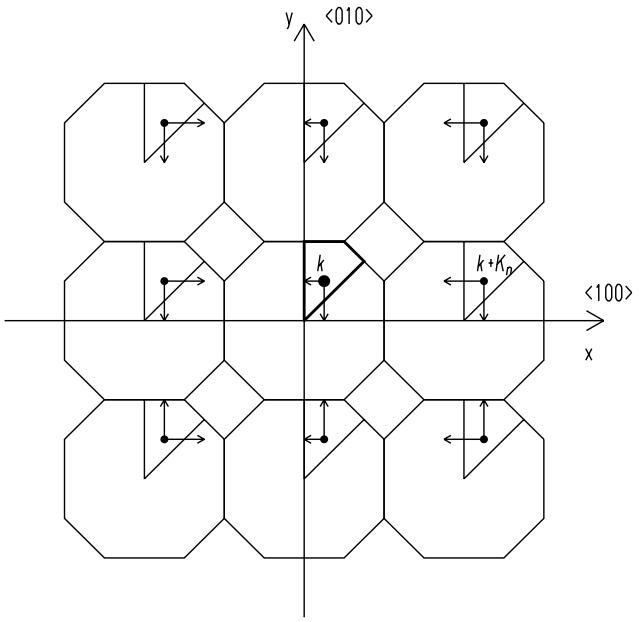

Figure 2. A (001) cross section of the repeated-zone scheme of the fcc Brillouin zone. The large dot denotes a $\boldsymbol{k}$-point in the first Brillouin zone and small dots denote $(\boldsymbol{k} + \boldsymbol{K}_n)$-points in the repeated zones. Arrows indicate the projection onto the x- or y-axis.

The value of the momentum density at a $\boldsymbol{q}$-point is added to the value at each array element for the three partial profiles $J_{(100)}(q)$, $J_{(010)}(q)$, and $J_{(001)}(q)$.

Compton profiles with the electron correlation correction are calculated from the equation

$$J(q_z) = \sum_b \int\int\int n(E)\rho_b(\boldsymbol{q}; E)\,\mathrm{d}q_x\,\mathrm{d}q_y\,\mathrm{d}E = \int n(E)J(q_z, E)\,\mathrm{d}E \tag{15}$$

where $n(E)$ is an energy-dependent occupation probability function defined later. In order to carry out the calculation of equation (15), energy-dependent Compton profiles $J(q_z, E_i)$ are first calculated from

$$J(q_z, E_i)\,\Delta E = \sum_b \int\int\int_{E_i-\Delta E}^{E_i} \rho_b(\boldsymbol{q}; E)\,\mathrm{d}q_x\,\mathrm{d}q_y\,\mathrm{d}E. \tag{16}$$

Here the value of ΔE is 0.022 Ryd. The calculation of the energy-dependent Compton profiles $J(q_z, E)$ is also performed using a similar procedure for the calculation of the IPM $J(q_z)$.

3. Results and discussion

The energy-dependent Compton profiles $J(q_z, E_i)$ of Al along the $\langle 100\rangle$, $\langle 110\rangle$, and $\langle 111\rangle$ directions, with convolution with a Gaussian of FWHM 0.1 au corresponding to the width of the resolution function for the experiment performed in reference [13], are shown in figure 3 together with that of the free-electron system $J(q_z, E)$.

The energy-dependent Compton profile $J(q_z, E)$ of the free-electron system is defined by differentiating the Compton profile with respect to energy E. As has been mentioned, the Compton profile of the free-electron system up to q_{max} is an inverted parabola:

$$J(q_z) \propto \begin{cases} q_{max}^2 - q_z^2 = E - q_z^2 & |q_z| \leqslant \sqrt{E} \\ 0 & |q_z| > \sqrt{E} \end{cases} \tag{17}$$

where $E = q_{max}^2$. Thus, the energy-dependent Compton profile of the free-electron system is reduced to

$$J(q_z, E) \propto \frac{\mathrm{d}J(q_z)}{\mathrm{d}E} = \begin{cases} 1 & |q_z| \leqslant \sqrt{E} \\ 0 & |q_z| > \sqrt{E}. \end{cases} \tag{18}$$

As seen from figure 3(a), the form of the energy-dependent Compton profiles is a totally flat plateau with a parabolic border that is a sharp cliff. On the plateau of the profile for Al, there is less structure in a region of lower energy and some structure around the Fermi energy, due to the BZ boundary effect. The structures in the profiles for the three directions differ from each other. When $J(q_z, E)$ is integrated along the energy axis from the bottom of the band to the Fermi energy, the conventional IPM Compton profile $J(q_z)$ is obtained. When $J(q_z, E)$ is integrated along the momentum axis, on the other hand, the density-of-states curve $N(E)$ is obtained. The Fermi energy E_F is determined to be 0.6493 Ryd from the density-of-states curve.

As usual, around the origin of the momentum axis the values of the IPM Compton profiles are a little greater than the experimental ones and in the higher-momentum region the opposite is true. In order to investigate the difference between theory and experiment, which is assumed to be due to the electron–electron correlation effect, an energy occupation function $n(E)$ is introduced which is similar to that introduced in reference [8]. The momentum occupation function $n(q)$ was first introduced by Daniel and Vosko [2]. In the electron gas system the energy E of an electron is proportional to the squared momentum q, i.e. $E \propto q^2$. We adopt

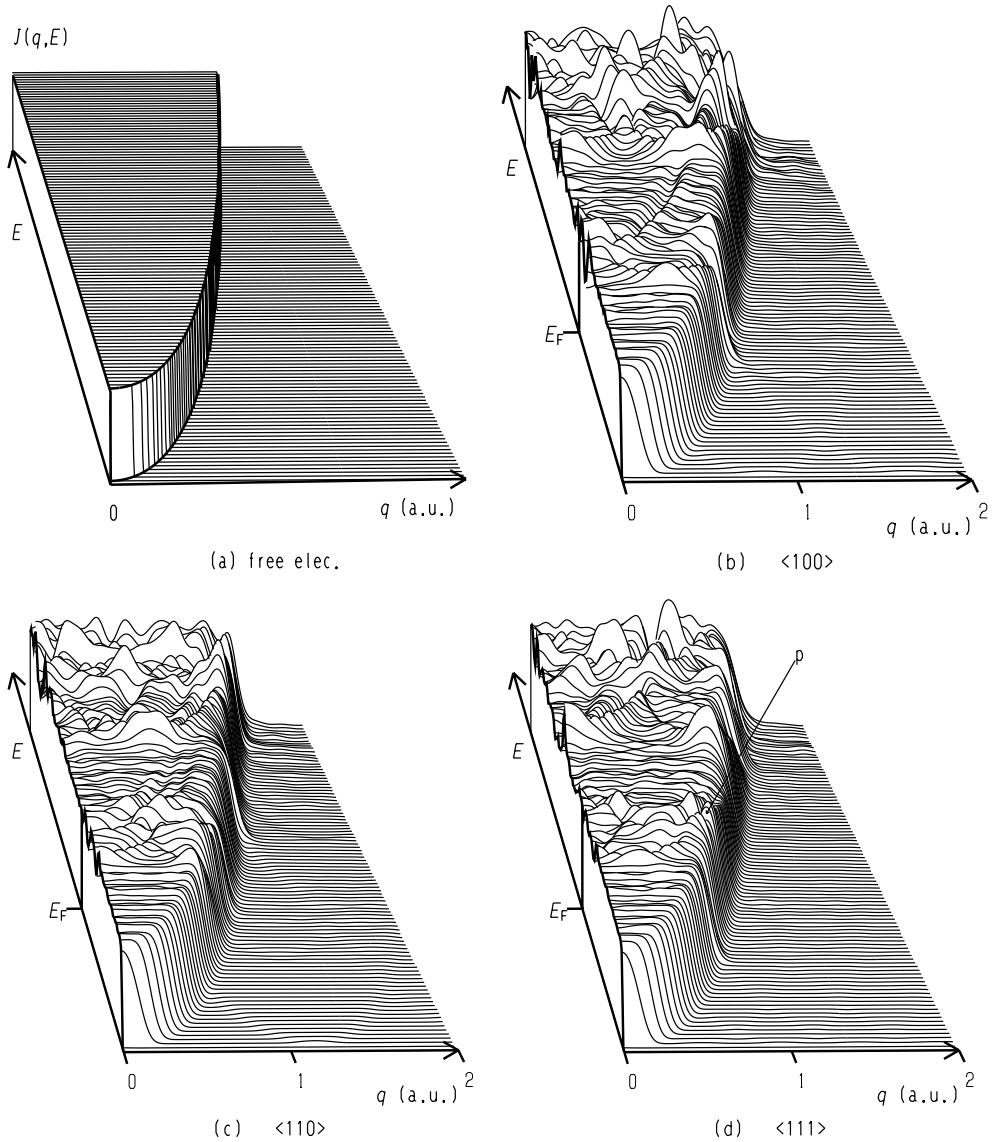

Figure 3. Energy-dependent Compton profiles $J(q_z, E)$. (a) shows those in a free-electron system. (b), (c), and (d) show those calculated from the band theory for Al along ⟨100⟩, ⟨110⟩, and ⟨111⟩ directions, respectively, convoluted with a Gaussian of FWHM 0.1 au. E_F denotes the Fermi energy.

the momentum occupation function $n(q)$ defined by Cardwell and Cooper [14] which is as follows:

$$n(q) = \begin{cases} 1 - aq^2/q_F^2 - d(1 - q/q_F) & q \leqslant q_F \\ a(q-b)^2/(q_F - b)^2 & q_F < q \leqslant b \\ 0 & b < q. \end{cases} \tag{19}$$

Substituting $q = \sqrt{E}$ into the above equation, we obtain the energy occupation function as

follows:

$$n(E) = \begin{cases} 1 - aE/E_{\mathrm{F}} - d(1 - \sqrt{E}/\sqrt{E_{\mathrm{F}}}) & E \leqslant E_{\mathrm{F}} \\ a(\sqrt{E} - \sqrt{E_{\mathrm{b}}})^2/(\sqrt{E_{\mathrm{F}}} - \sqrt{E_{\mathrm{b}}})^2 & E_{\mathrm{F}} < E \leqslant E_{\mathrm{b}} \\ 0 & E_{\mathrm{b}} < E. \end{cases} \tag{20}$$

As the electron-density parameter r_s of Al is 2.08 au, the values of a and d are estimated from the figures showing the momentum occupation function $n(q)$ given as figure 2 of reference [2] to be 0.16 and 0.03 respectively. E_{b} is the point at which $n(E)$ becomes zero and is determined from the following normalization condition:

$$\int_{\Gamma_1}^{E_{\mathrm{F}}} N(E)(1 - n(E))\,\mathrm{d}E = \int_{E_{\mathrm{F}}}^{E_{\mathrm{b}}} N(E)n(E)\,\mathrm{d}E \tag{21}$$

where Γ_1 denotes the energy at the bottom of the 4s band of Al, which is -0.1657 Ryd.

The density-of-states histogram calculated for the same energy values as were used to obtain the energy-dependent Compton profiles shown in figure 3 is shown in figure 4, together with the histogram of the energy occupation function $n(E)$ determined from it.

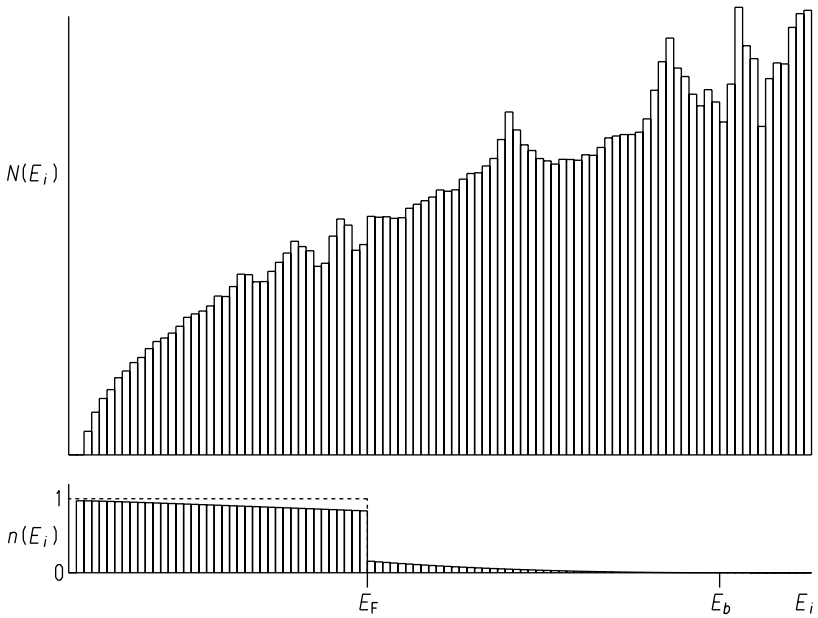

Figure 4. Histograms of the density of states $N(E)$ (at the top) and the energy occupation function $n(E)$ (at the bottom) for Al, i.e. for the electron-density parameter $r_s = 2.08$ au. E_{F} denotes the Fermi energy and E_{b} the point at which $n(E)$ becomes zero.

Γ_1 is situated at E_2, $E_{\mathrm{F}} = E_{39}$, and $E_{\mathrm{b}} = E_{84}$. Using the energy occupation function, the theoretical Compton profile with correlation correction is defined as follows:

$$J^{\mathrm{corr}}(q_z) = \sum_{i=1}^{n_{\max}} n(E_i)J(q_z, E_i)\,\Delta E. \tag{22}$$

In order to investigate the difference in detail, we show the differences between the experimental profile and the theoretical one without the correlation correction in figure 5 (as dots) together with the correlation-corrected theoretical profiles (as solid lines) which are

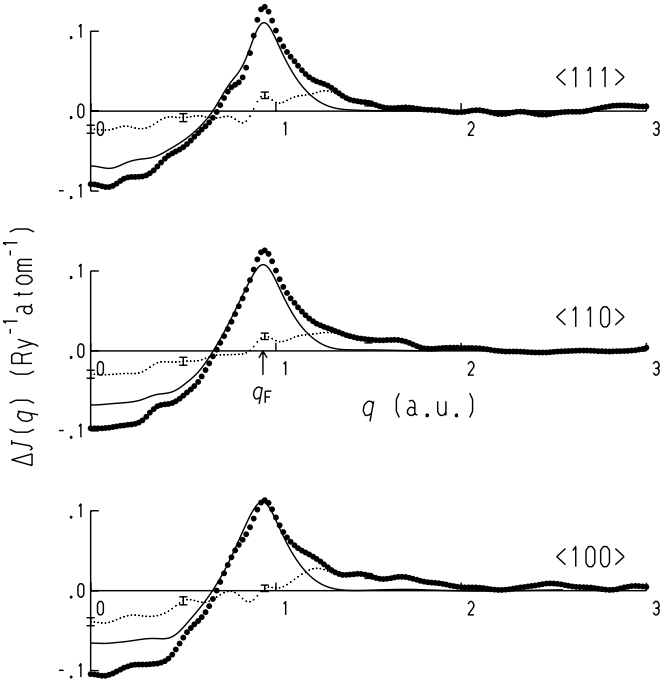

Figure 5. Profiles of the difference between experiment and the IPM (dots: $\Delta J^{(\mathrm{E-I})}$), the correlation-corrected results (solid lines: ΔJ^{corr}), and the difference between experiment and the theory with correlation correction (dotted lines: $\Delta J^{(\mathrm{E-C})}$), along three major axes. Some error bars of the experiment are shown by the symbols I.

defined as follows:

$$\Delta J^{\mathrm{corr}}(q_z) = J^{\mathrm{corr}}(q_z) - J(q_z) = -\sum_{\Gamma_1}^{E_{\mathrm{F}}} J(q_z, E)\,\Delta E\,(1 - n(E)) + \sum_{E_{\mathrm{F}}}^{E_{\mathrm{b}}} J(q_z, E)\,\Delta E\,n(E). \tag{23}$$

The differences between experiment and the theory with the correlation correction are also shown in figure 5 (as dotted lines). The agreement between experiment and theory is improved very much by introducing the correlation correction, but still some discrepancy remains. Comparing ΔJ^{corr} and $\Delta J^{(\mathrm{E-I})}$ it is seen that around the origin and in the higher-momentum region the magnitudes are different from each other, but the subtle structures are similar. As seen from the dotted curves $\Delta J^{(\mathrm{E-C})}$, the experimental values are still bigger in the higher-momentum region and smaller around the origin.

Figure 6 shows the directional difference for the Compton profile, $\langle 111\rangle - \langle 110\rangle$, together with that of the angular correlation of positron annihilation radiation taken from figure 8 in reference [4] for comparison. It is seen that below the Fermi momentum q_{F}, the correlation effect reduces the anisotropy remarkably and improves the agreement between theory and experiment very much. As seen from the figures, the difference curves have a concavity at a momentum value around 0.5 au and a sharp peak at around 0.85 au. The origin of the peak was discussed in reference [4]: it was ascribed to the Fermi surface geometry of fcc Al, especially around the L point. In figure 3(d) the source of the peak is indicated by p. The agreement between theory and experiment for the angular correlation is still better than that for the Compton profile.

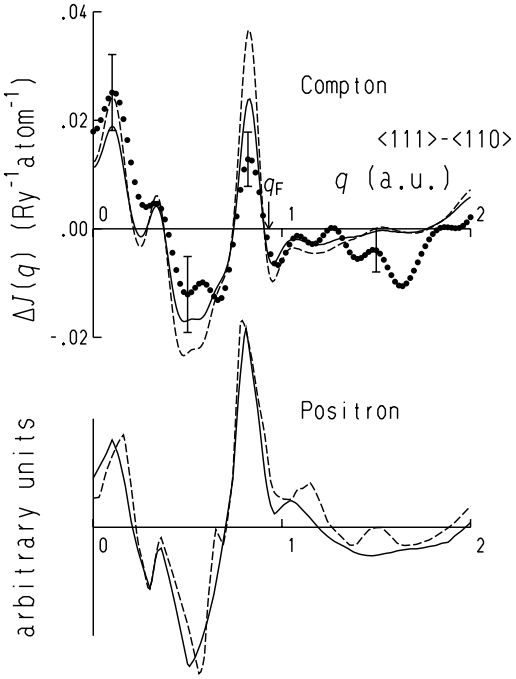

Figure 6. The directional difference for the Compton profile, $\langle 111\rangle - \langle 110\rangle$ (at the top), and that for the angular correlation of positron annihilation radiation (at the bottom). At the top, the dots denote the experimental values measured by Ohata [13], the dashed line is that for the IPM, and the solid line is that with correlation correction, with the electron-density parameter $r_s = 2.08$ au. Some error bars of the experiment are shown by the symbols I. At the bottom, the figure is taken from figure 8 in reference [4]. The solid line denotes the theory and the dashed one the experimental results.

If the experiment is precise enough and we need to achieve better agreement, there may be several possible ways to improve it. In order to reduce the difference between theory and experiment in figure 5:

(a) simply use a stronger correlation effect, i.e. use a bigger r_s-value;
(b) use the GW-approximation or one beyond the RPA (random-phase approximation) instead of using the phenomenological correlation effect;
(c) use a different core contribution which has smaller values around the origin and larger ones in the region of momentum above the Fermi momentum; or
(d) use some method beyond the impulse approximation or fully relativistic scattering theory.

In order to reduce the directional difference in figure 6:

(e) use the FLAPW programs.

In conclusion, we may say that we can almost reproduce the experimental Compton profiles for Al by taking into account the electron correlation effect phenomenologically, and the difference which still remains between theory and experiment should be discussed on the basis of more elaborate experiments and more reliable theory for the electron correlation effect.

Acknowledgments

We thank Dr T Ohata at Himeji Institute of Technology for sending us measured data prior to publication and Dr I Matsumoto at KEK for many helpful discussions.

References

[1] Stuewer R H and Cooper M J 1977 *Compton Scattering* ed B Williams (New York: McGraw-Hill) pp 1–27
[2] Daniel E and Vosko S H 1960 *Phys. Rev.* **120** 2041–4
[3] Lundqvist B I and Lyden C 1971 *Phys. Rev.* **4** 3360–70
[4] Kubo Y, Wakoh S and Yamashita J 1976 *J. Phys. Soc. Japan* **41** 830–5
[5] Lam L and Platzman P M 1974 *Phys. Rev.* B **9** 5122–7
[6] Rennert P 1981 *Phys. Status Solidi* **105** 567–75
[7] Rennert P, Carl G and Gläser U-H 1983 *Phys. Status Solidi* **115** 219–24
[8] Wakoh S and Matsumoto M 1990 *J. Phys.: Condens. Matter* **2** 797–807
[9] Kubo Y 1997 *J. Phys. Soc. Japan* **66** 2236–9
[10] Matsumoto M, Sano T and Wakoh S 1999 *J. Phys. Soc. Japan* **68** 1035–9
[11] Garreau Y and Loupias G 1990 *Solid State Commun.* **74** 583–7
[12] Sourtti P, Buslaps T, Honkimäki V, Metz C, Shukla A, Tschentscher Th, Kwiatkowska J, Maniawski F, Bansil A, Kaprzyk S, Kheifets A S, Lun D R, Sattler T, Schneider J R and Bell F 2000 *J. Phys. Chem. Solids* **61** 397–401
[13] Ohata T Private communication
[14] Cardwell D A and Cooper M J 1989 *J. Phys.: Condens. Matter* **1** 9357–67